New Journal of Physics
The open access journal at the forefront of physics

Deutsche Physikalische Gesellschaft DPG IOP Institute of Physics

PAPER • OPEN ACCESS

Time-resolved quantum spin transport through an Aharonov–Casher ring

To cite this article: Can Li *et al* 2018 *New J. Phys.* **20** 093023

New Journal of Physics
The open access journal at the forefront of physics

Deutsche Physikalische Gesellschaft DPG
IOP Institute of Physics

Published in partnership with: Deutsche Physikalische Gesellschaft and the Institute of Physics

OPEN ACCESS

RECEIVED
18 July 2018

REVISED
27 August 2018

ACCEPTED FOR PUBLICATION
7 September 2018

PUBLISHED
20 September 2018

PAPER

Time-resolved quantum spin transport through an Aharonov–Casher ring

Can Li[1], **Yaojin Li**[1], **Dongxing Yu**[1] **and Chenglong Jia**[1,2]

[1] Key Laboratory for Magnetism and Magnetic Materials of the Ministry of Education, Lanzhou University, Lanzhou 730000, People's Republic of China
[2] Institut für Physik, Martin-Luther Universität Halle-Wittenberg, Halle (Saale), D-06099, Germany

E-mail: cljia@lzu.edu.cn

Keywords: spin transport, Aharonov–Casher effect, spin–orbit interaction, interference effect, spin precession

Abstract

After obtaining an exact analytical time-varying solution for the Aharonov–Casher conducting ring embedded in a textured static/dynamic electric field, we investigate the spin-resolved quantum transport in the structure. It is shown that the interference patterns are governed by not only the Aharonov–Casher geometry phase but also the instantaneous phase difference of spin precession through different traveling paths. This dynamic phase is determined by the strength of the applied electric field and can have substantial effects on the charge/spin conductances, especially in the weak field regime as the period of spin precession comparable to that of the orbital motion. Our studies suggest that a low-frequency normal electric field with moderate strength possesses more degrees of freedom for manipulating the spin interference of incident electrons.

Introduction

How to control and engineer the spin degree of freedom at the mesoscopic scale is a crucial step for spintronic devices [1–7]. It has been demonstrated that spins of conduction electrons can be manipulated by external gating voltage through the Rashba spin–orbit interaction (RSOI) [8–15]. Such the electric field-tunable RSOI can be achieved as well on the Aharonov–Casher (AC) effect [16] in mesoscopic ring structures [17–19]. Electron wave that traverses the AC ring along clockwise and counterclockwise directions accumulates different phases, which is reflected in the spin interference patterns of the conductance. By measuring interference patterns, the phase difference can be detected experimentally. In particular, a spin geometric phase, which is robust against the spin dephasing, can be distinguished [20, 21]. However, it should be noted that the spinor wavefunctions used to investigate the spin interference effects in experiment and theory are *not* time-dependent even though the spin precession in quantum transport is always there. The tilt angle between the *mean* axis of the spin precession and the normal direction to the ring plane has been used to characterize the conductance [22–24].

In the present study, we revisit the AC ring in the presence of static/dynamic electric fields. By giving an exact solution for traversing electrons at time t, a time-resolved spin precession is identified. We show that the interference patterns are determined by not only the AC phase but also the instantaneous phase difference of spin precessions through different traveling paths. Especially, such the time-resolved phase difference becomes more pronounced as the strength and the frequency of the applied electric field decrease. The spin conductivity and the bulk spin polarization (which describes the spin-dependent electronic transport in the ring) are found to be strongly depend on the spin polarization orientation of incident electrons. Our results show that the AC ring can act as a spin interferometer, but the electric field should be properly adjusted to optimize the spin interference effects.

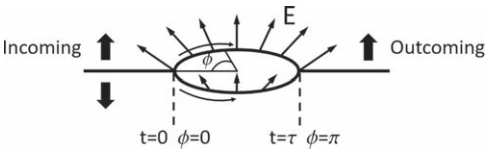

Figure 1. Schematic of a quantum AC ring symmetrically coupled to two leads in the presence of electric field **E**. A symmetrically textured electric field is assumed for the sake of theoretical investigation as that in the [23].

Time-varying wavefunction

Let us begin with the Hamiltonian for electrons with effective mass M confined to a ring of radius a under a (time-dependent) textured electric field $\mathbf{E}(t) = E_r(t)\hat{\mathbf{e}}_r + E_z(t)\hat{\mathbf{e}}_z$ (see figure 1)[3]

$$H = \frac{1}{2M}\left(\mathbf{P}_\phi - \frac{\mu}{2c}\boldsymbol{\sigma} \times \mathbf{E}\right)^2 = \frac{\mathbf{L}_z^2}{2Ma^2} + \frac{\mu \mathbf{L}_z}{2Mac}(\sigma_r E_z - \sigma_z E_r), \tag{1}$$

where we have introduced the polar angle ϕ in cylindrical coordinates and $\mathbf{L}_z = -\mathrm{i}\hbar\partial/\partial\phi$. σ_i (with $i = r,\ \phi,\ z$) are the spin Pauli operators that satisfy the commute relation $[\hat{\sigma}_i,\ \hat{\sigma}_j] = 2\mathrm{i}\epsilon_{ijk}\hat{\sigma}_k$, and $\mu = e\hbar/2Mc$ is the magnetic moment. $E_r(t)$ and $E_z(t)$ are assumed to be ϕ-independent. The system then possesses the cylindrical symmetry, i.e., $[\mathbf{L}_z,\ H] = 0$, which leads to the conservation of orbital angular momentum. Consequently, the invariant subspace can be labeled by certain eigenvalue n of $\mathbf{L}_z$ and the non-autonomous Hamiltonian becomes a linear function of the σ_i,

$$H = \frac{\hbar\omega_0}{2}n^2 + \frac{\hbar\omega_r}{2}\sigma_r - \frac{\hbar\omega_z}{2}\sigma_z \tag{2}$$

with $\omega_0 = \frac{\hbar}{Ma^2}$, $\omega_z = \frac{\mu n}{Mac}E_r$, and $\omega_r = \frac{\mu n}{Mac}E_z$. To solve the Schrödinger equation, $\mathrm{i}\hbar\frac{\partial}{\partial t}|\Psi(t)\rangle = H|\Psi(t)\rangle$ without specifying the time-dependence of electric field $\mathbf{E}(t)$, we perform a gauge transformation [25, 26]

$$U_g(t) = \exp[\mathrm{i}v_z(t)\sigma_z]\exp[\mathrm{i}v_\phi(t)\sigma_\phi], \tag{3}$$

$$H \to \tilde{H} = U_g^{-1}HU_g - \mathrm{i}\hbar U_g^{-1}\partial U_g/\partial t, \tag{4}$$

$$|\Psi(t)\rangle \to |\tilde{\Psi}(t)\rangle = U_g^{-1}|\Psi(t)\rangle. \tag{5}$$

Under the best gauge conditions

$$2\frac{\mathrm{d}v_\phi}{\mathrm{d}t} + \omega_r \sin 2v_z = 0,$$
$$\omega_r \cos 2v_\phi \cos 2v_z + \omega_z \sin 2v_\phi + 2\frac{\mathrm{d}v_z}{\mathrm{d}t}\sin 2v_\phi = 0, \tag{6}$$

we have then the diagonalized gauge Hamiltonian in the $\tilde{\sigma}_z$ representation

$$\tilde{H} = \frac{\hbar\omega_0}{2}n^2 - \frac{\hbar}{2}\frac{\omega_r \cos 2v_z}{\sin 2v_\phi}\tilde{\sigma}_z. \tag{7}$$

Let $|m\rangle$ be the eigenstate of $\tilde{\sigma}_z$ with eigenvalue $m(= \pm 1)$, the solution of the gauged Schrödinger equation can be written explicitly as

$$|\tilde{\Psi}_{n,m}(\phi,\ t)\rangle = \mathrm{e}^{-\mathrm{i}\Theta_{n,m}(t)}\mathrm{e}^{\mathrm{i}n\phi}|m\rangle \tag{8}$$

with $\Theta_{n,m}(t) = \frac{1}{\hbar}\int_0^t \tilde{E}_{n,m}(t')\mathrm{d}t'$ and $\tilde{E}_{n,m}(t) = \frac{\hbar\omega_0}{2}n^2 - \frac{m\hbar}{2}\frac{\omega_r \cos 2v_z}{\sin 2v_\phi}$ being the energy eigenvalue of the gauge Hamiltonian $\tilde{H}$. Based on the gauge transformation $|\Psi(t)\rangle = U_g|\tilde{\Psi}(t)\rangle$, the real time spin-resolved solution of the original Schrödinger equation reads then

$$|\Psi_{n,m}(\phi,\ t)\rangle = \mathrm{e}^{-\mathrm{i}\Theta_{n,m}(t)}\mathrm{e}^{\mathrm{i}n\phi}\sum_{m'} D^{1/2}_{mm'}(v_\phi,\ v_z)\mathrm{e}^{\mathrm{i}m'v_z}|m'\rangle, \tag{9}$$

[3] The correction term that contains σ_ϕ is neglected in the case of large angular momentum.

where

$$D^{1/2}[\nu_\phi(t),\ \nu_z(t)] = \begin{bmatrix} \cos\nu_\phi(t) & \sin\nu_\phi(t)e^{2i\nu_z(t)} \\ -\sin\nu_\phi(t)e^{-2i\nu_z(t)} & \cos\nu_\phi(t) \end{bmatrix} \tag{10}$$

is the Wigner function. The energy of the system is given by

$$E_{n,m}(t) = \frac{\hbar\omega_0}{2}n^2 - \frac{m\hbar}{2}(\omega_r \sin 2\nu_\phi \cos 2\nu_z - \omega_z \cos 2\nu_\phi). \tag{11}$$

It is easy to check that $|\Psi_{n,m}(\phi,\ t)\rangle$ are complete and orthogonal in the whole Hilbert space. The general wavefunction of the ring can thus be expanded as, $|\Psi(\phi,\ t)\rangle = \sum_{n,m} C_{n,m}|\Psi_{n,m}(\phi,\ t)\rangle$, where $C_{n,m}$ are time-independent coefficients and completely determined by the initial conditions. It is worthy to note that $|\Psi_{n,m}(\phi,\ t)\rangle$ is quite general for the AC ring with any cylindrical symmetric electric field $\mathbf{E}(t)$. In particular, $|\Psi_{n,m}(\phi,\ t)\rangle$ can describe precisely and advantageously the spin precession in a static electric field (see below). From the best gauge conditions, equation (6) with the initial values $\nu_\phi(0)$ and $\nu_z(0)$, the time-varying $\nu_\phi(t)$ and $\nu_z(t)$ can be worked out, and then all the properties of the system should be obtained.

To get a clear insight into the physical meanings of $\nu_\phi(t)$ and $\nu_z(t)$, let us write down the expected value of spin vector $\langle\boldsymbol{\sigma}\rangle$ by using the basis $|\Psi_{n,m}(\phi,\ t)\rangle$,

$$\langle\sigma_z\rangle = m\cos 2\nu_\phi(t), \tag{12}$$

$$\langle\sigma_r\rangle = -m\sin 2\nu_\phi(t)\cos 2\nu_z(t), \tag{13}$$

$$\langle\sigma_\phi\rangle = m\sin 2\nu_\phi(t)\sin 2\nu_z(t), \tag{14}$$

which indicate that $\nu_\phi(t)$ describes the *instantaneous* tilt angle from the normal z-direction at time t and $\nu_z(t)$ characterizes the spin rotation angle around the z-axis. In figure 2, we plot $\langle\sigma_z\rangle$ and $\langle\sigma_r\rangle$ versus the magnitude E of a *static* normal electric field $\mathbf{E} = E\hat{\mathbf{e}}_z$ (here it should be noted that the energy $E_{n,m}$ is time-independent even though $\nu_\phi(t)$ and $\nu_z(t)$ are time-varying under the static electric field). As one can see that $\langle\sigma_r\rangle$ is time-independent, satisfying the conservation equation $[\sigma_r,\ H] = 0$. When the strength E of normal electric fields is enhanced, $\langle\sigma_z\rangle$ (and $\langle\sigma_\phi\rangle$) becomes oscillating precessionally with the time t, which is quite different from the previous (theoretical) spinor wavefunctions that deduce a time-independent expected value of $\langle\boldsymbol{\sigma}\rangle$ once the electric field $\mathbf{E}$ is given [22, 23]. One can also notice in figure 2 that, as the normal electric field is enhanced, the spin precession becomes faster and the precession axis tends to follow the direction of the effective magnetic field (along the radial direction).

Quantum spin transport

Based on the wavefunction $|\Psi_{n,m}(\phi,\ t)\rangle$, now we consider a ring symmetrically coupled to two equivalent contact leads (see figure 1). In clear comparison to the spin interference patterns given by time-independent spinor wavefunctions with the mean axis of the spin precession [22, 23], a perfect coupling between leads and ring is assumed (i.e., fully transparent contacts and no backscattering effects) to the first order linear approximation. Given an incident electron with energy E_F and spin $|s\rangle = C_\uparrow|\uparrow\rangle + C_\downarrow|\downarrow\rangle$ ($\sum_m C_m^2 = 1$) from the left lead, depending on the spin alignment (m) and the direction of angular momentum (counterclockwise or clockwise with $\lambda = \pm 1$, respectively), the initial electronic state in the ring at $\phi = 0$ and $t = 0$ becomes a superposition of the four wavefunctions $|\Psi_{n_m^\lambda,m}(0,\ 0)\rangle = \sum_{m'} C_m D^{1/2}_{mm'}[\nu_\phi(0),\ \nu_z(0)]|m'\rangle$, where n_m^λ is determined by solving $E_F = E_{n_m^\lambda,m}(0)$ in equation (11) and does not require to be integer. Then, the incoming spin $|s\rangle$ entering the ring at $\phi = 0$ propagate precessionally along the four Feynman paths and interfere at $\phi = \pi$ after time τ. To this end, we calculate the quantum probability of transmission for the outgoing spin $|s'\rangle$ channel

$$T_{s'} = |\sum_{n_m^\lambda,m} \langle s'|\Psi_{n_m^\lambda,m}(\pi,\ \tau)\rangle|^2. \tag{15}$$

The zero-temperature charge and spin conductances are given, respectively, by the Landauer formula [27]

$$G_c = \frac{e^2}{h}(T_\uparrow + T_\downarrow) \text{ and } G_s = \frac{e^2}{h}(T_\uparrow - T_\downarrow). \tag{16}$$

The corresponding bulk spin polarization is defined by $P_z = G_s/G_c$ [28]. Clearly, we have now two important but separated time scales: the Larmor frequency of spin precession and the frequency of orbital revolution around the ring. By carrying out the tedious but straightforward algebra, we find the modulation of conductances origins indeed from the phase difference (acquired by different Feynman paths), which is however a composite of two terms as well: (i) the spin geometric phase accumulated by the change of spinor orientation during transport that is determined by the mean spin precession angle, and (ii) the instantaneous spin precession phase difference $\Delta\nu_z$ at $\phi = \pi$ and $t = \tau$ through different traveling paths.

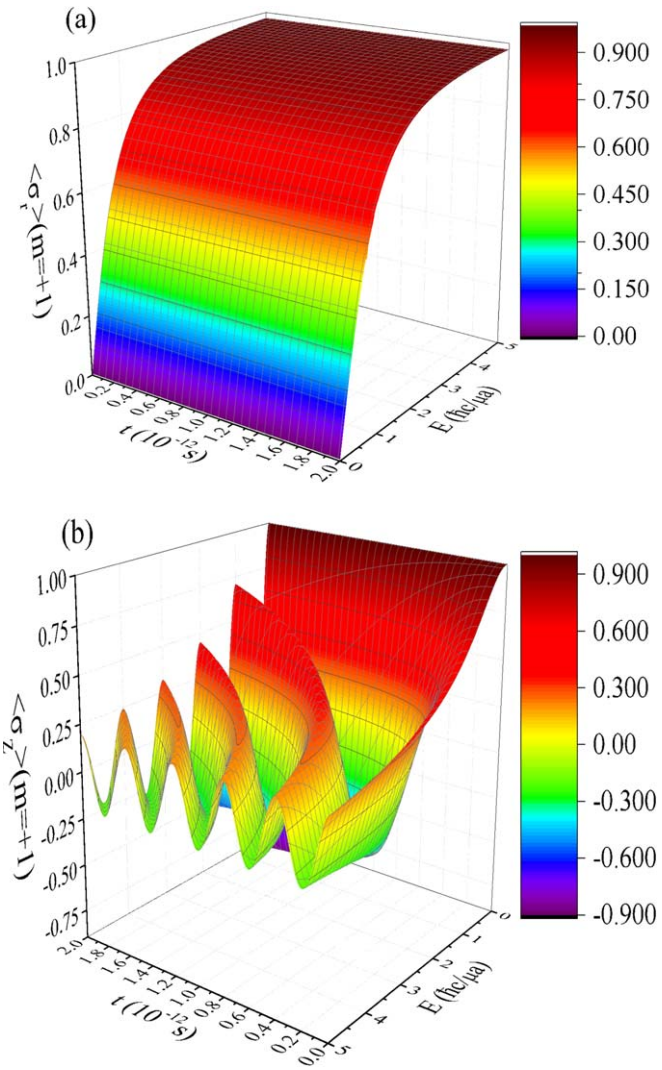

Figure 2. Dynamical evolution of the spin state: (a) $\langle\sigma_r\rangle$ and (b) $\langle\sigma_z\rangle$, respectively, in the AC ring subjected to a *static* electric field $\mathbf{E} = E\hat{\mathbf{e}}_z$. The initial conditions are $\nu_\phi(0) = -1/2\arctan(\mu Ea/\hbar c)$ and $\nu_z(0) = 0$.

Firstly, let us try to reproduce the charge conductance, for instance that in [22], based on equations (15) and (16) by using the wavefunction $|\Psi_{n,m}(\phi,\ t)\rangle$, but with a presupposed *time-independent* tilt angle $\nu_\phi(0) = -\frac{1}{2}\arctan\frac{\mu Ea}{\hbar c}$ [22, 23]. The numerical results are shown in figure 3 by the dash–dot line, which is in good agreement with the analytical expression in the adiabatic limit (i.e., the Larmor frequency of spin precession is much large than the frequency of orbital revolution), $G_c = \frac{e^2}{h}[1 - \cos(\pi\sqrt{1 + Q_R^2})]$ with $\tan 2\nu_\phi = Q_R$. Here Q_R representing the RSOI constant that has the same effect as the normal electric field E_z in the AC ring. However, after consistently solving the coupled differential equations equation (6) with the initial conditions $\nu_\phi(0) = -\frac{1}{2}\arctan\frac{\mu Ea}{\hbar c}$ and $\nu_z(0) = 0$ (at $\phi = 0$), we find that, as the electric field E_z decreases, (i) the mean axis of the spin precession tends to align itself in the normal direction of the ring plane and thus the associated spin solid angle becomes smaller; (ii) whereas, the instantaneous spin-resolved phase difference $\Delta\nu_z(\tau)$ at $\phi = \pi$ becomes more pronounced in weak electric field area, as the spin has a comparable precession period to its orbital motion and the spin dephasing induced by the (fast) spin precession is strongly suppressed (see the figure 3(b)). As a result, the adiabatic condition is broken and the dynamical modulation effect of spin precession gets enhanced and the charge conductance possesses substantial deviation from the values only with the AC geometry phase (see figure 3(a)). On the other hand, in the presence of strong electric fields, for example the experimental set up in [20, 21], the spin precession is accelerated (see figure 2) and the instantaneous phase difference $\Delta\nu_z(\tau)$ becomes small and even random. The interference effect of the charge conductance is dominated again by the AC phase. Such time-resolved spin precession effect also demonstrates itself in the spin transport behavior. As shown in figures 4(a), depending on the spin state of the incident electron, the spin-dependent transmission changes dramatically: one gets a large spin resistance for fully *spin-polarized* incoming

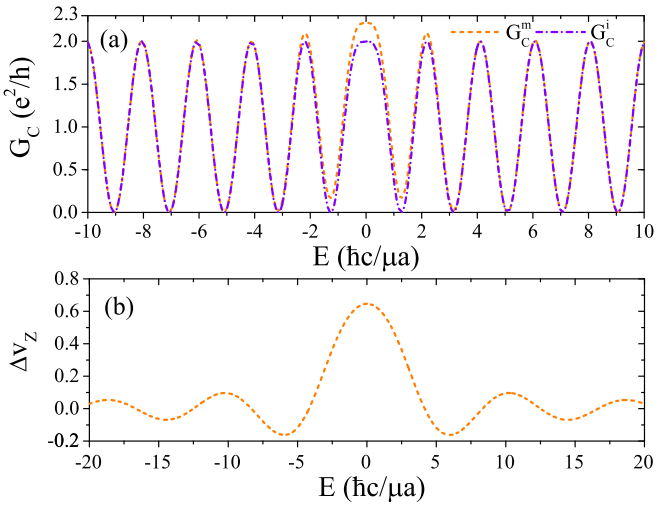

Figure 3. The charge conductance with presupposed time-independent tilt angle v_ϕ (G_c^i with dash–dot line) or self-consistently solved v_ϕ (G_c^m with dash line) as a function of the strength E of normal electric field. The dash–dot curve shows good consistency with the results in [22] except the area near $E = 0$. The instantaneous spin precession phase differences Δv_z at $\phi = \pi$ and $t = \tau$ are shown below as the function of E. Here the incoming energy is $E_F = 5$ eV.

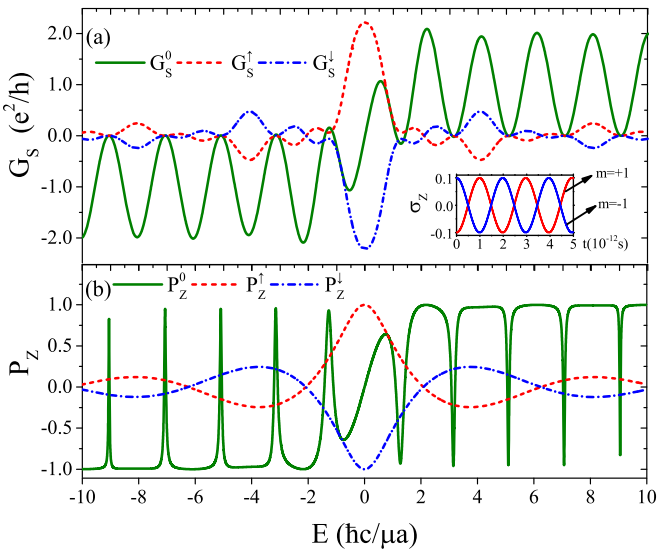

Figure 4. Numerical results for the spin conductance and the spin polarization by using the time-varying wavefunction equation (9). G_s^0 (P_z^0), $G_s^\uparrow$ ($P_z^\uparrow$), and $G_s^\downarrow$ ($P_z^\downarrow$) correspond to the different incident spin state, $C_\uparrow = C_\downarrow = \sqrt{2}/2$, $C_\uparrow = 1$ but $C_\downarrow = 0$, and $C_\uparrow = 0$ but $C_\downarrow = 1$, respectively. The inset shows the time evolution of $\langle\sigma_z\rangle$ ($m = \pm 1$) with $E = 10\ \hbar c/\mu a$. Here, $E_F = 5$ eV, $v_\phi(0) = -1/2 \arctan(\frac{\mu E a}{\hbar c})$, and $v_z(0) = 0$.

electron (i.e., nearly zero $G_s^\uparrow$ and $G_s^\downarrow$ in most areas of electric fields except $|E_z| < 1\ \hbar c/\mu a$), but the similar AC oscillations of the spin conductance of the spin *un-polarized* incident electron. Furthermore, figures 4(a) clearly indicates that the spin polarization of the incoming electron in the AC ring can be tuned by the normal electric field (see also figures 4(b)). Unfortunately, the weakest RSOI realized experimentally in [20] was $Q_R = 0.25$, corresponding to $E = 0.35\ \hbar c/\mu a$ in our case, which is slightly higher than the point that the non-adiabatic deviations become noticeable in figures 3. We expect a weaker RSOI to emphasize the spin precession effect in the non-adiabatic regime in experiments.

The effect of an in-plane electric field is studied by tuning the tilt angle γ of a textured electric field $\mathbf{E} = E(\cos\gamma\hat{\mathbf{e}}_r + \sin\gamma\hat{\mathbf{e}}_z)$. It is clear that one cannot change the spin polarization orientation of incident z-polarized electron by the AC ring in the presence of in-plane field E_r only, being consistent with the constraint condition $[\sigma_z, H] = 0$ under $\gamma = 0$. However, as shown in figure 5, the angle γ is capable of controlling the modulation of polarization of electron transmitted.

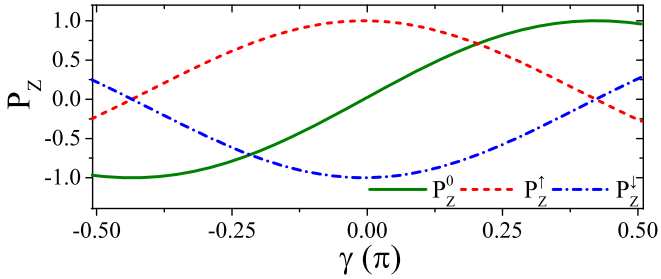

Figure 5. The influence of the in-plane component of the textured electric field $\mathbf{E} = E(\cos\gamma\hat{\mathbf{e}}_r + \sin\gamma\hat{\mathbf{e}}_z)$ on the spin polarization. The amplitude $E = 4\ \hbar c/\mu a$ is fixed during the numerical calculation.

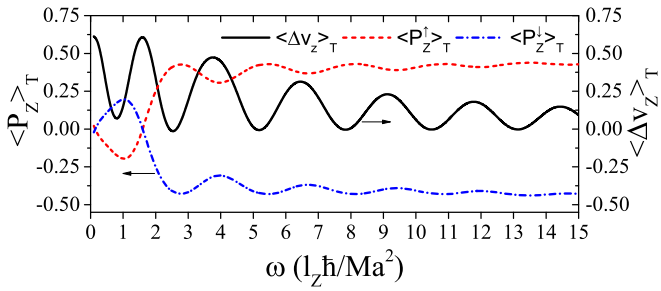

Figure 6. Dynamic effects of the AC electric field $\mathbf{E}(t) = E\cos(\omega t + \Phi)\hat{\mathbf{e}}_z$ on the integral-averaged spin polarization. The amplitude of the applied electric field is $E = 5\ \hbar c/\mu a$ and the incoming energy reads $E_F = 5$ eV.

To complete the discussion of dynamic effects we investigate in the following an AC normal electric field $\mathbf{E}(t) = E\cos(\omega t + \Phi)\hat{\mathbf{e}}_z$. Considering that not a single electron but an electron current is injected into the ring, the *effective* initial phase Φ seen by each individual incident electrons at the left incoming contact changes continuously with time, which would result in a periodic modulation in the outgoing transmission with respected to the time (equivalently, the phase Φ). Therefore, we take the time integral of charge/spin conductances over a period interval $2\pi/\omega$. It is found that the integral-averaged spin polarization $\langle P_z\rangle$ of unpolarized incoming electron current is zero. However, the numerical results reveal that the AC field is helpful to improve the spin interference effect of the fully spin-polarized incoming electrons (see figure 6). Due to the dynamic phase difference Δv_z, the spin polarizations oscillate with the frequency of applied AC fields and tend to be stabilized in the high frequency region.

Conclusion

In conclusion, for the quantum spin transport through an AC ring in the presence of cylindrical electric fields, we have presented an exact time-dependent solution for the problem by using the algebra dynamic method and focus on the time-resolved spin interference effect. It is revealed that, besides the spin geometry phase, the instantaneous phase different of spin precession in different Feynman paths has big influence on the interference patterns in the case of weak and/or low-frequency electric fields. We have also demonstrated the possibility to control the spin polarization by the frequency, the strength, and the tilt angle of applied electric field. Our time-dependent solutions are general and can be applied to the AC ring based spintronic devices with any type of rotationally textured electric fields. In the non-ballistic regime, especially in the presence of significant disorder, the momentum scattering reorients the direction of the spin precession axis resulting in a random effective electric field and dynamic phase difference, which would lead to an average spin dephasing.

Acknowledgments

This work is supported by the National Natural Science Foundation of China (No. 11474138 and No. 11834005), the German Research Foundation (No. SFB 762), the Program for Changjiang Scholars and Innovative Research Team in University (No. IRT-16R35), and the Fundamental Research Funds for the Central Universities.

References

[1] Fiederling R, Keim M, Reuscher G, Ossau W, Schmidt G, Waag A and Molenkamp L W 1999 *Nature* **402** 787
[2] Motsnyi V F, Safarov V I, De Boeck J, Das J, Van Roy W, Goovaerts E and Borghs G 2002 *Appl. Phys. Lett.* **81** 265
[3] Popp M, Frustaglia D and Richter K 2003 *Nanotechnology* **14** 347
[4] van't Erve O M J, Kioseoglou G, Hanbicki A T, Li C H, Jonker B T, Mallory R, Yasar M and Petrou A 2004 *Appl. Phys. Lett.* **84** 4334
[5] Tosi L and Aligia A A 2011 *Phys. Status Solidi* b **248** 732–40
[6] Jonker B T, Kioseoglou G, Hanbicki A T, Li C H and Thompson P E 2007 *Nat. Phys.* **3** 542
[7] Suzuki T, Sasaki T, Oikawa T, Shiraishi M, Suzuki Y and Noguchi K 2011 *Appl. Phys. Express* **4** 023003
[8] Mishchenko E G, Shytov A V and Halperin B T 2004 *Phys. Rev. Lett.* **93** 226602
[9] Nitta J, Meijer F E and Takayanagi H 1999 *Appl. Phys. Lett.* **75** 695
[10] Balatsky A V and Altshuler B L 1993 *Phys. Rev. Lett.* **70** 1678
[11] Choi M Y 1993 *Phys. Rev. Lett.* **71** 2987
[12] Lucignano P, Giuliano D and Tagliacozzo A 2007 *Phys. Rev.* B **76** 045324
[13] Zhu Z, Wang Y, Xia K, Xie X C and Ma Z 2007 *Phys. Rev.* B **76** 125311
[14] Souma S and Nikolić B K 2004 *Phys. Rev.* B **70** 195346
[15] Bercioux D and Lucignano P 2015 *Rep. Prog. Phys.* **78** 106001
[16] Aharonov Y and Casher A 1984 *Phys. Rev. Lett.* **53** 319
[17] Joibari F K, Blanter Y M and Bauer G E W 2013 *Phys. Rev.* B **88** 115410
[18] Bergsten T, Kobayashi T, Sekine Y and Nitta J 2006 *Phys. Rev. Lett.* **97** 196803
[19] Nitta J and Bergsten T 2007 *New J. Phys.* **9** 341
[20] Nagasawa F, Takagi J, Kunihashi Y, Kohda M and Nitta J 2012 *Phys. Rev. Lett.* **108** 086801
[21] Nagasawa F, Frustaglia D, Saarikoski H, Richter K and Nitta J 2013 *Nat. Commun.* **4** 2526
[22] Frustaglia D and Richter K 2004 *Phys. Rev.* B **69** 235310
[23] Shen S Q, Li Z J and Ma Z S 2004 *Appl. Phys. Lett.* **84** 996
[24] Richter K 2012 *Physics* **5** 1224
[25] Wang S J and Zuo W 1994 *Phys. Lett.* A **196** 13
[26] Jia C L, Wang S J, Luo H G and An J H 2004 *J. Phys.:Condens. Matter* **16** 2043
[27] Landauer R 1957 *IBM J. Res. Dev.* **1** 223
[28] Schmidt G 2005 *J. Phys. D: Appl. Phys.* **38** R107